

Particle Swarm Optimization for broadband energy harvesting of ambient mechanical vibrations

Original

Particle Swarm Optimization for broadband energy harvesting of ambient mechanical vibrations / Bonnin, M., Song, K., Traversa, F.L., Bonani, F.. - In: IEEE ACCESS. - ISSN 2169-3536. - ELETTRONICO. - (2025), pp. 193719-193731. [10.1109/access.2025.3631589]

Availability:

This version is available at: 11583/3005350 since: 2025-11-22T15:38:25Z

Publisher:

IEEE

Published

DOI:10.1109/access.2025.3631589

Terms of use:

This article is made available under terms and conditions as specified in the corresponding bibliographic description in the repository

Publisher copyright

(Article begins on next page)

RESEARCH ARTICLE

Particle Swarm Optimization for Broadband Energy Harvesting of Ambient Mechanical Vibrations

MICHELE BONNIN¹, KAILING SONG¹, (Member, IEEE), FABIO L. TRAVERSA²,
AND FABRIZIO BONANI¹, (Senior Member, IEEE)

¹Department of Electronics and Telecommunications, Politecnico di Torino, 10129 Turin, Italy

²MemComputing Inc., San Diego, CA 92121, USA

Corresponding author: Michele Bonnin (michele.bonnin@polito.it)

ABSTRACT We investigate a networked energy harvester designed to capture ambient dispersed mechanical vibrations modeled as white Gaussian noise. The system consists of coupled mechanical resonators and a piezoelectric transduction mechanism, forming a structure conceptually analogous to a mechanical filter, which can be optimized for broadband energy harvesting. By leveraging mechanical-to-electrical analogies, we develop an equivalent circuit model of the harvester and employ a transmission matrix method to derive analytical formulas for the transfer function, output voltage, average harvested power, and power efficiency in the frequency domain. The optimization of the harvester's performance is also addressed. Due to the lack of closed-form expressions for the objective function and its derivatives, we utilize gradient-free, swarm intelligence methods—specifically, Particle Swarm Optimization and Flock of Starling Optimization—to determine the optimal network parameters that maximize the output power over a wide frequency spectrum. Our results show that, with proper optimization, the networked energy harvester can deliver an output power increased by more than 100% with respect to a conventional single-degree-of-freedom harvester. We also find that increasing the number of mass-spring pairs yields diminishing advantages. Notably, the optimized harvester behaves as a broadband mechanical filter, trading peak resonance power for enhanced performance over a wider frequency range. Finally, we demonstrate that broadband optimization using Particle Swarm Optimization outperforms analytical strategies based on traditional impedance matching at resonance.

INDEX TERMS Energy harvesting, equivalent circuits, particle swarm optimization, stochastic processes.

I. INTRODUCTION

Energy harvesting (EH) refers to a set of technologies to realize micro-electro-mechanical systems capable of self-powering, or at least self-recharging their internal battery, by scavenging energy dispersed in the surrounding environment that would otherwise be wasted. EH is crucial in sustainable development and climate change mitigation, by promoting energy efficiency and enabling cleaner, more sustainable technologies. Reducing reliance on nonrenewable energy sources, EH contributes to lower the carbon footprint, and thus to create a more sustainable energy

mix. EH also contributes to the sustainable development goals eliminating, or at least extending, the lifespan of batteries, thus reducing hazardous electronic waste [1], [2].

EH is predicted to play a significant role in areas like sensor and actuator networks, wearable devices, and smart city infrastructure, where remote and difficult to access positioning make battery replacement costly and problematic. EH may also be beneficial for the Internet of Things, which demands low-power, long-lived, miniaturized electronic devices, where batteries may not be the ideal solution as long as they remain bulky and heavy [3], [4], [5].

The available sources for energy scavenging are diverse and abundant, including solar and wind power, thermal

The associate editor coordinating the review of this manuscript and approving it for publication was Jenny Mahoney.

gradients [6], [7], dispersed electromagnetic radiation [8], [9], and ambient mechanical vibrations [10].

An energy harvester for ambient mechanical vibrations must include an oscillating structure to capture vibration kinetic energy, and a transducer, to convert the kinetic energy into electrical power [11]. The oscillating structure can be modeled as a mass-spring system, possibly including a dampener accounting for dissipation effects. The mass-spring system represents a mechanical resonator characterized by its resonant frequency, where the oscillating amplitude, and consequently the scavenged power, is maximum. Around resonance, power collection performance rapidly degrades as frequency changes, implying that, if the energy of ambient vibrations is distributed over a wide frequency interval, only a limited portion of the available energy is actually harvested.

Several experimental implementations based on the aforementioned structure have been developed, leveraging diverse designs of mechanical oscillators. Notable recent advancements include energy harvesters for mechanical vibrations that utilize cantilever beam oscillators with piezoelectric transduction, incorporating features such as multi-stability [12], nonlinear stiffness [13], and hybrid piezoelectric-electromagnetic transduction [14]. Alternative oscillator designs include spherical pendulums [15], diaphragms [16], and arrays of piezoelectric harvesters optimized for wind-induced vibrations [17].

To maximize the scavenged power, the bandwidth around the resonant frequency should be as wide as possible, while at the same time maintaining the maximum amplitude sufficiently high [18], [19]. This is a classic problem in electronic engineering, strictly related to the design of broadband filters. In order to avoid power consumption, passive filters are the better solution. They are constructed using only passive components such as resistors, capacitors, and inductors, arranged in specific configurations to achieve the desired frequency response. A typical broadband passive filter can be realized using a ladder topology, consisting of cascade-connected L-sections.

Interestingly, ladder networks have a mechanical equivalent: i.e. a chain of masses connected pairwise through elastic springs. This suggests the idea of designing a multi degree-of-freedom, or networked, energy harvester, based on coupled mass-spring pairs, that can be designed as a mechanical filter and optimized to scavenge maximum power available in the surrounding environment. The use of additional mechanical degrees of freedom allows to improve the power conversion efficiency without involving electrical matching networks, which in some cases may require the use of large inductances that, in turn, easily become unpractical both for their possible value, and for their physical size.

In this work, we consider a networked energy harvester based on coupled resonators. Although our analysis is purely mathematical, we remark that the model is suitable for describing architectures that have been proposed and experimentally realized in recent years. In [20], the authors considered two harvesters coupled by a metallic rod,

exploiting rotational and translational displacements. In [21], a two degrees-of-freedom structure was proposed using two cantilevers, one with length l_1 and a second with length l_2 cut inside the first one. In [22] a magnetic coupling between two cantilevers was introduced by tip magnets, showing that magnetic interaction is equivalent to a coupling through a spring. Similar arrangements were considered in [23], [24], and [25].

Analogously to electrical filters, the networked harvester can be designed to pass a wide frequency interval, without hindering the maximum amplitude too much. The chain operates as a matching network [26], [27], [28], acting on the mechanical domain instead of the electrical one. The main advantage of using a mechanical filter is that the network with optimal parameters (masses and spring elastic constants) is easier to realize in practice. By contrast, previously proposed solutions based on the application of impedance matching require rather large inductance values, difficult to realize, to match the large impedance mismatch between the mechanical and the electrical part [29], [30].

The optimization of circuits and structures for broadband filtering and electromagnetic wave absorption is a complex and increasingly significant challenge. In recent years, swarm intelligence algorithms and metaheuristic approaches based on swarm intelligence have gained prominence in the field of electromagnetics, owing to their versatility and effectiveness in navigating complex, multimodal search spaces [31], [32]. In this work, we apply a swarm intelligence algorithm to optimize the mechanical resonating structure subject to the mechanical vibrations modeled as a white Gaussian noise.

As the main contribution, we demonstrate that after proper optimization the networked energy harvester scavenges more than 100% additional power compared to a simple, single mechanical degree-of-freedom energy harvester. We show that increasing the number of mass-spring pairs beyond three offers negligible returns in terms of increased scavenged power. Finally, we demonstrate that broadband optimization using swarm intelligence algorithms achieve superior performance compared to analytical methods based on broadband impedance matching calculated at a specific frequency.

This paper is organized as follows: In section II we describe the model of the energy harvester based on coupled mechanical resonators, and we derive the governing equations. In section III we use mechanical-to-electrical analogies to derive the equivalent circuit for the harvester. Section IV is dedicated to the analysis of the equivalent circuit. Using the transmission matrix formalism, we derive analytical formulas for the average harvested power and the power efficiency. In section V we describe the optimization of the harvester, based on Particle Swarm Optimization and Flock of Starling Optimization. Numerical results referring to a practical application are discussed in section VI. A comparison with conventional broadband filter design at a specific frequency is also made. Finally, section VII is devoted to conclusions.

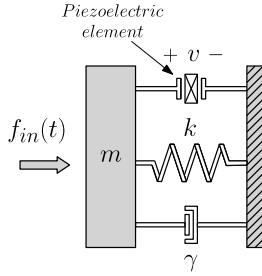


FIGURE 1. Schematic representation of a single mechanical degrees of freedom energy harvester for ambient vibrations.

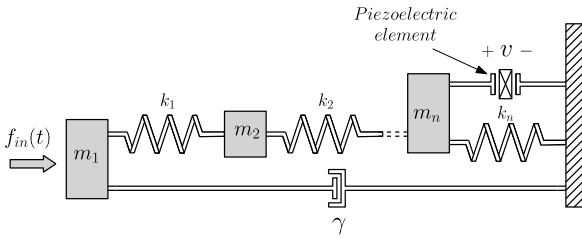


FIGURE 2. Schematic representation of a multi DoF energy harvester for ambient vibrations.

II. ENERGY HARVESTER MODELING

A. MECHANICAL DOMAIN MODELING

The mechanical part of the harvester is designed to resonate with the external force, and thus it can schematically be represented as a mechanical resonator (Fig. 1). The resonator is composed by a mass m connected to a transducer through an elastic spring with elastic constant k . Internal dissipation is accounted for by a dampener, with damping constant γ . The mechanical system is subject to two forces, the external (input) force $f_{in}(t)$, modeling ambient vibrations, and the force $f_{tr}(v)$ (where v is the voltage across the load), describing the action of the transducer on the resonator.

The equation of motion for the mass is readily derived from Fig. 1 as the balance of the applied forces, obtaining [33], [34]:

$$m \frac{d^2x}{dt^2} + \gamma \frac{dx}{dt} + kx = f_{in}(t) - f_{tr}(v) \quad (1)$$

where x is the mass displacement from the resting position. Single degree-of-freedom (DoF) dynamical systems of this type have been extensively studied and applied, both theoretically and experimentally, to model piezoelectric energy harvesters in linear [1], [18], [35] and nonlinear [9], [11], [15], [19] regimes.

In this work we consider a generalization of the aforementioned model, in the form of a broadband mechanical resonator composed by a chain of masses connected pairwise by elastic springs (Fig. 2). Without too much loss of generality, we assume that dissipation effects are negligible, except for the first mass of the chain.

Through the balance of the forces applied to each mass, we obtain the governing equations of motion:

$$m_1 \frac{d^2x_1}{dt^2} + \gamma \frac{dx_1}{dt} + k_1(x_1 - x_2) = f_{in}(t) \quad (2a)$$

$$m_2 \frac{d^2x_2}{dt^2} + k_1(x_2 - x_1) + k_2(x_2 - x_3) = 0 \quad (2b)$$

⋮

$$m_n \frac{d^2x_n}{dt^2} + k_{n-1}(x_n - x_{n-1}) + k_n x_n = -f_{tr}(v) \quad (2c)$$

where x_j is the displacement of the j -th mass from the resting position, and k_j is the stiffness of the j -th spring. System (2) can be conveniently rewritten in the compact form

$$\begin{aligned} m_j \frac{d^2x_j}{dt^2} + k_{j-1}(x_j - x_{j-1}) + k_j(x_j - x_{j+1}) + \gamma \frac{dx_j}{dt} \delta_{j1} \\ = f_{in}(t) \delta_{j1} - f_{tr}(v) \delta_{jn} \end{aligned} \quad (3)$$

where $k_0 = 0$, $x_0 = x_{n+1} = 0$, and δ_{ij} is the Kronecker delta function.

Alternatively, the governing equations (2) can be rewritten as the system of first order differential equations:

$$\frac{dx_j}{dt} = y_j \quad (4a)$$

$$\begin{aligned} \frac{dy_j}{dt} = -\frac{k_{j-1}}{m_j}(x_j - x_{j-1}) - \frac{k_j}{m_j}(x_j - x_{j+1}) \\ + \frac{1}{m_j} (f_{in}(t) - \gamma y_j) \delta_{j1} - \frac{f_{tr}(v)}{m_j} \delta_{jn} \end{aligned} \quad (4b)$$

for $j = 1, \dots, n$.

B. PIEZOELECTRIC TRANSDUCER

Different transduction mechanisms can be exploited to convert mechanical energy into electrical power, including electromagnetic induction [36], [37], [38], [39], [40], [41], [42], magnetostrictive phenomena [43], [44], [45] and electrostatic conversion [46]. Piezoelectric transducers are particularly interesting, because they are relatively low cost, easy to manufacture and to miniaturize [2], [47], [48], [49], [50], [51]. Typically, the coupling between the mechanical and the electrical domains is weak enough, that the coupling force can be assumed linear. As an example, we consider the constitutive equations for a linear piezoelectric material [52]:

$$\begin{bmatrix} S \\ D \end{bmatrix} = \begin{bmatrix} s^E & d \\ d^T & \epsilon^T \end{bmatrix} \begin{bmatrix} T \\ E \end{bmatrix} \quad (5)$$

where S and T are the mechanical strain and stress tensors, D and E are the dielectric displacement and electric field vectors, s^E and d are the compliance (evaluated at constant electric field) and the piezoelectric charge constants tensors, while ϵ^T is the absolute permittivity evaluated at constant stress [53].



FIGURE 3. Two-port representation of the piezoelectric transducer.

Through spatial integration of the microscopic description (5), a lumped parameter model describing the macroscopic behavior in terms of the force f_{tr} , displacement x of the mass connected to the transducer, charge q and voltage v , can be derived. In the quasi-static regime, neglecting the stiffness of the piezoelectric material, the governing equations are:

$$f_{tr}(t) = -\alpha v(t) \tag{6a}$$

$$q(t) = \alpha x(t) - C_{pz} v(t) \tag{6b}$$

where α is the electro-mechanical coupling (in N/V or As/m), and C_{pz} is the capacitance of the transducer.

System (6) describes the electro-mechanical two port shown in Fig. 3. At the left port the effort variable is the force $f_{tr}(t)$, and the flux variable is the velocity $dx(t)/dt$. At the right port, the effort is the voltage $v(t)$ and the flux is the current $i(t) = dq(t)/dt$.

Taking the derivatives in (6b) and assuming that the load can be modeled as a resistor with conductance G_L we obtain:

$$\frac{dv}{dt} = \frac{\alpha}{C_{pz}} \frac{dx}{dt} - \frac{G_L}{C_{pz}} v \tag{7}$$

III. EQUIVALENT CIRCUIT

Mechanical-electrical analogies are powerful methods to translate electrical systems into mechanical systems and vice versa, making easier to transfer concepts and solutions from one domain to the other. Historically, mechanical-electrical analogies were introduced in the XIX century, to translate the relatively new electromagnetic phenomena into the more familiar mechanical ones. Today, they remain useful because they allow to use lumped circuit models to represent electro-mechanical systems, making frequency domain analysis easier, and simplifying the design of systems with prescribed transfer functions.

In the impedance analogy, masses are replaced by inductors, springs by capacitors, dampeners by resistors and forces by voltage sources. Using the substitutions summarized in table 1, the state equations (4) and (7) become:

$$\frac{dq_j}{dt} = i_j \tag{8a}$$

$$\begin{aligned} \frac{di_j}{dt} = & -\frac{1}{L_j C_{j-1}}(q_j - q_{j-1}) - \frac{1}{L_j C_j}(q_j - q_{j+1}) \\ & + \frac{1}{L_j} (v_{in}(t) - R i_j) \delta_{j1} - \frac{1}{n_t L_j} v \delta_{jn} \end{aligned} \tag{8b}$$

TABLE 1. Mechanical-electrical analogy.

Mechanical	Electrical
Force, f	Voltage, v
Displacement, x	Charge, q
Momentum $m\dot{x}$	Flux linkage, φ
Mass, m	Inductance L
Compliance, k^{-1}	Capacity, C
Damping, γ	Resistance, R

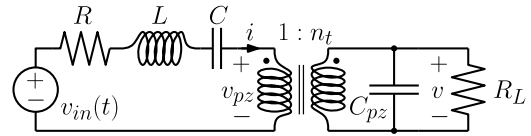


FIGURE 4. Equivalent circuit for a single mass-spring pair energy harvester for ambient mechanical vibrations.

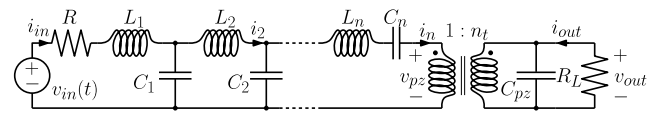


FIGURE 5. Equivalent circuit for a multiple mass-spring pairs energy harvester for ambient mechanical vibrations.

$$\frac{dv}{dt} = \frac{1}{n_t C_{pz}} i_n - \frac{G_L}{C_{pz}} v \tag{8c}$$

where $n_t = \alpha^{-1}$ is the turns ratio of the ideal transformer.

From the system of differential equations (8), it is easy to derive the equivalent circuit for the energy harvester. Figures 4 and 5, show the equivalent circuits for the energy harvester with one and n mass-spring pairs, respectively.

The force generated by ambient mechanical vibrations is represented by the voltage source. For random vibrations, the voltage $v_s(t)$ is a white Gaussian noise, and equations (8) becomes a system of stochastic differential equations. Notice that because the noise is additive (or un-modulated), the stochastic equation can be interpreted indifferently as Itô or Stratonovich. We will interpret all stochastic differential equations as Itô. The chain of mass-spring pairs is represented by the ladder of electrical resonators, composed by L-connected inductor and capacitor pairs. Note that the last inductor and capacitor pair are series connected, to represents the fact that the last mechanical resonator is directly connected to the transducer. The ladder is a filter with Cauer topology, that can be optimized to allow maximum energy transfer. Finally, the piezoelectric transducer is represented by an ideal transformer, responsible for transferring energy from the mechanical domain to the electrical load, modeled by the resistor R_L . The capacitive behavior of piezoelectric material is taken into account by the capacitor C_{pz} connected in parallel with the electrical load.

IV. ANALYSIS

A linear time invariant (LTI) system is characterized by its input-output relationship:

$$y(t) = \int_{-\infty}^{+\infty} h(r)x(t-r) dr = h(t) * x(t) \quad (9)$$

where $h(t)$ is the impulse response, $x(t)$, $y(t)$ are the input and the output signals, respectively, and $*$ denotes convolution. The autocorrelation function $R_{yy}(\tau)$ of the output variable $y(t)$ is given by [54]:

$$\begin{aligned} R_{yy}(\tau) &= E[y(t)y(t-\tau)] \\ &= \int_{-\infty}^{+\infty} \int_{-\infty}^{+\infty} h(r)h(s)R_{xx}(\tau+r-s) ds dr \end{aligned} \quad (10)$$

where $E[\cdot]$ denotes the expectation. Taking the Fourier transform yields the relationship between the input and the output power spectral densities (PSDs):

$$S_Y(\omega) = |H(\omega)|^2 S_X(\omega) \quad (11)$$

where $H(\omega) = \hat{Y}(\omega)/\hat{X}(\omega)$ is the transfer function, and $\hat{Y}(\omega)$, $\hat{X}(\omega)$ are the Fourier transforms of the output and the input signals, respectively. The total power is calculated by integrating the correspondent power spectral densities over the whole frequency spectrum.

We assume that the mechanical vibrations can be modeled as a white Gaussian noise, i.e. the formal derivative of a Wiener process:

$$v_{in}(t) = D \frac{dW_t}{dt} \quad (12)$$

The Wiener process W_t is characterized by zero expectation $E[W_t] = 0$, covariance $E[W_t W_s] = \min(t, s)$ and a centered normal distribution $W_t \sim \mathcal{N}(0, t)$. Using the Wiener-Khinchin theorem [54], the PSD for the white Gaussian noise can be calculated as the Fourier transform of the correlation function, thereby obtaining:

$$S_{V_{in}}(\omega) = D^2 \quad (13)$$

The constant PSD described by (13), clearly shows that white Gaussian noise is an idealization, because it would imply that vibrations carry an infinite amount of energy. Nevertheless, white Gaussian noise remains a useful model for those processes characterized by relatively wide energy spectrum.

Using (11) and (13), the average harvested power becomes:

$$P_{G_L} = G_L E[v^2(t)] = \frac{D^2}{2\pi} G_L \int_{-\infty}^{+\infty} |H(\omega)|^2 d\omega \quad (14)$$

where $H(\omega) = \hat{V}_{out}(\omega)/\hat{V}_{in}(\omega)$ is the transfer function.

Similarly, the average power injected by the noise in the harvester is

$$P_{in} = E[v_{in}(t) i_{in}(t)] = \frac{D^2}{2\pi} \int_{-\infty}^{+\infty} \text{Re}[Y(\omega)] d\omega \quad (15)$$

where $Y(\omega) = \hat{I}_{in}(\omega)/\hat{V}_{in}(\omega)$ is the input admittance, and $\text{Re}[\cdot]$ denotes the real part.

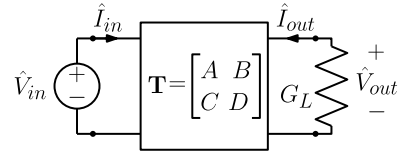


FIGURE 6. LTI two-port network closed on a resistor with conductance $G_L = R_L^{-1}$.

The efficiency of the harvester is

$$\eta = \frac{P_{G_L}}{P_{in}} = G_L \frac{\int_{-\infty}^{+\infty} |H(\omega)|^2 d\omega}{\int_{-\infty}^{+\infty} \text{Re}[Y(\omega)] d\omega} \quad (16)$$

The transfer functions can be easily calculated using the transmission matrix. For the LTI, two-port network shown in Fig. 6, the transmission or $ABCD$ matrix $\mathbf{T}(\omega)$ defines the relationships between the input and output quantities:

$$\begin{aligned} \begin{bmatrix} \hat{V}_{in}(\omega) \\ \hat{I}_{in}(\omega) \end{bmatrix} &= \mathbf{T}(\omega) \begin{bmatrix} \hat{V}_{out}(\omega) \\ -\hat{I}_{out}(\omega) \end{bmatrix} \\ &= \begin{bmatrix} A(\omega) & B(\omega) \\ C(\omega) & D(\omega) \end{bmatrix} \begin{bmatrix} \hat{V}_{out}(\omega) \\ -\hat{I}_{out}(\omega) \end{bmatrix} \end{aligned} \quad (17)$$

For the resistive load of Fig. 6, $\hat{I}_{out} = -G_L \hat{V}_{out}$, that substituted in (17) yields

$$H(\omega) = \frac{\hat{V}_{out}}{\hat{V}_{in}} = (A(\omega) + B(\omega)G_L)^{-1} \quad (18a)$$

$$Y(\omega) = \frac{\hat{I}_{in}}{\hat{V}_{in}} = \frac{C(\omega) + D(\omega)G_L}{A(\omega) + B(\omega)G_L} \quad (18b)$$

The transmission matrix can be efficiently calculated using the peculiar structure of the equivalent circuit shown in Fig. 5. Given a network composed by $n+1$ cascade connected two-ports, each one described by a transmission matrix $\mathbf{T}_k(\omega)$, the total transmission matrix is:

$$\mathbf{T}(\omega) = \prod_{k=1}^{n+1} \mathbf{T}_k(\omega) \quad (19)$$

The stage transmission matrices \mathbf{T}_k are calculated as follows. Fig. 7 shows the equivalent circuit for the first stage of the energy harvester, i.e. the first mass-spring pair and the dampener. Using Kirchhoff current and voltage laws (KCL and KVL), the transmission matrix for the first stage is easily found as:

$$\mathbf{T}_1 = \begin{bmatrix} 1 + j\omega RC_1 + (j\omega)^2 L_1 C_1 & R + j\omega L_1 \\ j\omega C_1 & 1 \end{bmatrix} \quad (20)$$

where $j = \sqrt{-1}$.

Similarly, Fig. 8 shows the equivalent circuit for the k -th mass-spring pair, with $k = 2, \dots, n-1$. Using KVL and KCL the transmission matrix is:

$$\mathbf{T}_k = \begin{bmatrix} 1 + (j\omega)^2 L_k C_k & j\omega L_k \\ j\omega C_k & 1 \end{bmatrix} \quad (21)$$

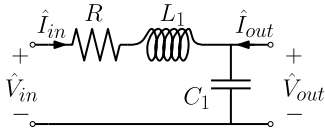


FIGURE 7. Equivalent circuit for the first stage of the energy harvester, corresponding to the dampener and the first mass-spring pair.

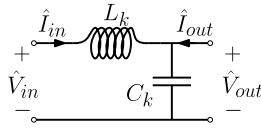


FIGURE 8. Equivalent circuit for the intermediate mass-spring stages.

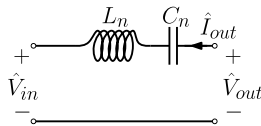


FIGURE 9. Equivalent circuit for the last mass-spring pair.

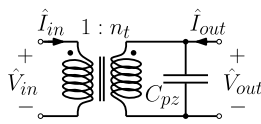


FIGURE 10. Equivalent circuit for the piezoelectric transducer.

The equivalent circuit for the last stage of the mass-spring chain is shown in Fig. 9, with the corresponding transmission matrix

$$\mathbf{T}_n = \begin{bmatrix} 1 & j\omega L_n + \frac{1}{j\omega C_n} \\ 0 & 1 \end{bmatrix} \quad (22)$$

Finally, Fig. 10 shows the equivalent circuit for the piezoelectric transducer. Using KVL/KCL and the constitutive relationships of the ideal transformer leads to the transmission matrix

$$\mathbf{T}_{n+1} = \begin{bmatrix} 1/n_t & 0 \\ j\omega n_t C_{pz} & n_t \end{bmatrix} \quad (23)$$

Using (18)-(23), the transfer function for a networked energy harvester composed by an arbitrary number of mass-spring pairs is easy to derive. The transfer function is then introduced into (14) to calculate the average scavenged power.

V. PARTICLE SWARM OPTIMIZATION OF THE NETWORKED HARVESTER

In this section we consider the problem of the optimization of the networked structure. We assume that the values of some parameters, summarized in table 2, are fixed, and using the equivalent circuit and the results of section IV, we design the mechanical filter that maximizes the harvested energy. We use the single DoF energy harvester shown in Fig. 1, with

TABLE 2. Values of the equivalent circuit's parameters used in the analysis.

Parameter	Value
R	0.12Ω
D	10^{-3} V
$n_t = \alpha^{-1}$	238.0952
L_n	10 mH
C_n	1 mF
C_{pz}	80.08 nF
R_L	10 k Ω

the equivalent circuit of Fig. 4, as a benchmark, to assess the advantages offered by the networked architecture.

We denote with $\boldsymbol{\mu} = [L_1, \dots, L_{n-1}, C_1, \dots, C_{n-1}]^T$ the vector of the energy harvester's parameters, and with $S \subset \mathbb{R}^{2n-2}$ the parameter space. To make the comparison fair, we use fixed values for the last inductance L_n and the last capacitance C_n , equal to the values of L and C used for the one DoF harvester. The optimization problem is the following: Find

$$\boldsymbol{\mu}^* = \arg \max_{\boldsymbol{\mu} \in S} P_{G_L} \quad (24)$$

Since P_{G_L} is obtained by solving the integral equation (14), closed-form analytical expressions for the harvested power and its derivatives are not available. Consequently, gradient-based optimization methods – whether first- or higher-order – are ill-suited for this problem.

Swarm intelligence refers to a class of meta-heuristic algorithms widely used for solving complex optimization tasks efficiently. Over 500 meta-heuristic algorithms have been proposed to date, with more than 350 introduced in the past decade alone [55]. This rapid growth has raised questions about overlapping concepts among algorithms presented under different names. Well-known examples of meta-heuristics include Particle Swarm Optimization (PSO), inspired by the collective behavior of bird flocks or fish schools; Genetic Algorithms, inspired by natural selection; Simulated Annealing, based on the annealing process in metallurgy; and Ant Colony Optimization, which mimics how ants find shortest paths.

Although many gradient-free methods could in principle address our optimization problem, PSO is particularly well suited due to its demonstrated effectiveness and reliability when the objective function must be evaluated numerically.

PSO offers several advantages for our problem. As a gradient-free algorithm, it does not require derivative information. It is simple to implement, requires minimal parameter tuning, and is inherently parallelizable – a rather beneficial feature when function evaluations involve costly numerical integration. Its population-based structure enables broad exploration of the search space while also effectively converging toward promising solutions through social learning mechanisms.

The original PSO algorithm was introduced in [56]. In its standard version, a swarm of N particles explores the parameter space seeking for the global minimum/maximum of the fitness function [57]. Each particle position μ_i and the corresponding velocity v_i are initialized at random, and for each iteration the best position that has been found for particle i is denoted as $\mathbf{p}_{i,\text{best}}$, while the best position that has been found for the whole swarm is denoted as \mathbf{g}_{best} . Each particle's velocity and position are updated according to:

$$v_i(t+1) = w v_i(t) + c_1 r_1 (\mathbf{p}_{i,\text{best}}(t) - \mu_i(t)) + c_2 r_2 (\mathbf{g}_{\text{best}}(t) - \mu_i(t)) \quad (25a)$$

$$\mu_i(t+1) = \mu_i(t) + v_i(t+1) \quad (25b)$$

for all $i = 1 \dots N$. Here w is the inertial weight, the hyper-parameters c_1 and c_2 are the cognitive and social acceleration coefficients, and $r_1, r_2 \in [0, 1]$ are two uniformly distributed random variables.

To avoid divergence, the velocity is bounded to a maximum v_{max} . In components:

$$v_i^{(k)}(t+1) = \min(v_i^{(k)}(t+1), v_{\text{max}}^{(k)}) \quad (26)$$

Analogously, the position can be constrained, introducing boundaries to the parameter space P . Let μ_{min} and μ_{max} be the vectors of the lower and upper bounds, respectively, then

$$\mu_i^{(k)}(t+1) = \max(\min(\mu_i^{(k)}(t+1), \mu_{\text{max}}^{(k)}), \mu_{\text{min}}^{(k)}) \quad (27)$$

PSO terminates either after reaching a predefined maximum number of iterations or function evaluations, preventing the search from running indefinitely, or based on convergence criteria. One common convergence condition occurs when the improvement in the global best solution falls below a small threshold over a certain number of consecutive iterations, suggesting that the swarm has likely found an optimal or near-optimal solution and further search may not yield meaningful gains. This is detected by monitoring stagnation over T_{stagnant} consecutive steps. Specifically, stagnation is identified by observing the change in the global best fitness value $f(\mathbf{g}_{\text{best}})$; if the improvement between successive iterations is less than a threshold ϵ , a stagnation counter s increments. When an improvement greater than ϵ occurs, the counter resets to zero. Consequently, the algorithm can terminate early if no significant progress is made for a specified number of iterations, ensuring efficient convergence while avoiding unnecessary computations once progress stalls [58].

The main computational advantage of PSO is that it can easily be parallelized. Large swarms of particles can be used to explore the parameter space, and the position and the velocity of each particle can be updated independently from, and in parallel with, all the others. The personal best and the global best can be updated only once per iteration. Another positive aspect of PSO is that it offers an excellent balance between exploration, which is the tendency to explore regions of the parameter space not visited before,

Algorithm 1 PSO Algorithm With Convergence-Based Termination condition for the Optimization of the Networked Energy Harvester

Input : $\mu_i(1), v_i(1)$, initial guess for position (parameters) and velocity.

Output: $\mathbf{g}_{\text{best}} = \mu^* = \arg \max \sigma^*(\mu)$.

- 1 Initialize the swarm size n_s and the number of dimensions
- 2 Set values for hyper-parameters: c_1, c_2, w (inertia weight)
- 3 Set maximum number of iterations and initialize iteration counter $t = 1$
- 4 Set convergence threshold ϵ and maximum stagnation steps T_{stagnant}
- 5 Initialize stagnation counter $s = 0$ and previous best value $f_{\text{prev}} = \infty$
- 6 **for each particle** $i \in [1, n_s]$ **do**
 - 7 Randomly generate $\mu_i(1)$ and $v_i(1)$
 - 8 Evaluate: $f(\mu_i(1)) = -P_{G_L}(\mu_i(1))$
 - 9 Set $\mathbf{p}_{\text{best},i} = \mu_i(1)$ and $f(\mathbf{p}_{\text{best},i}) = f(\mu_i(1))$
- 10 **end**
- 11 Set $\mathbf{g}_{\text{best}} = \mathbf{p}_{\text{best},1}$ and $f(\mathbf{g}_{\text{best}}) = f(\mathbf{p}_{\text{best},1})$
- 12 **for each particle** $i \in [1, n_s]$ **do**
 - 13 **if** $f(\mathbf{p}_{\text{best},i}) < f(\mathbf{g}_{\text{best}})$ **then**
 - 14 $\mathbf{g}_{\text{best}} = \mathbf{p}_{\text{best},i}$
 - 15 $f(\mathbf{g}_{\text{best}}) = f(\mathbf{p}_{\text{best},i})$
 - 16 **end**
- 17 **end**
- 18 **while** $t < \text{maximum number of iterations}$ **and** $s < T_{\text{stagnant}}$ **do**
 - 19 **for each particle** $i \in [1, n_s]$ **do**
 - 20 Update velocity: $v_i(t+1) = w v_i(t) + c_1 r_1 (\mathbf{p}_{\text{best},i} - \mu_i(t)) + c_2 r_2 (\mathbf{g}_{\text{best}} - \mu_i(t))$
 - 21 Update position: $\mu_i(t+1) = \mu_i(t) + v_i(t+1)$
 - 22 Apply boundaries to $\mu_i^{(k)}$ and $v_i^{(k)}$
 - 23 Evaluate: $f(\mu_i(t+1)) = -P_{G_L}(\mu_i(t+1))$
 - 24 **if** $f(\mu_i(t+1)) < f(\mathbf{p}_{\text{best},i})$ **then**
 - 25 $\mathbf{p}_{\text{best},i} = \mu_i(t+1)$
 - 26 $f(\mathbf{p}_{\text{best},i}) = f(\mu_i(t+1))$
 - 27 **end**
 - 28 **if** $f(\mathbf{p}_{\text{best},i}) < f(\mathbf{g}_{\text{best}})$ **then**
 - 29 $\mathbf{g}_{\text{best}} = \mathbf{p}_{\text{best},i}$
 - 30 $f(\mathbf{g}_{\text{best}}) = f(\mathbf{p}_{\text{best},i})$
 - 31 **end**
 - 32 **end**
 - 33 **if** $|f(\mathbf{g}_{\text{best}}) - f_{\text{prev}}| < \epsilon$ **then**
 - 34 $s = s + 1$
 - 35 **end**
 - 36 **else**
 - 37 $s = 0$
 - 38 **end**
 - 39 $f_{\text{prev}} = f(\mathbf{g}_{\text{best}})$
 - 40 $t = t + 1$
- 41 **end**
- 42 **return** \mathbf{g}_{best}

and exploitation, which is the contrary tendency to focus on promising regions [57]. For an overview about the pros and cons of PSO and a detailed comparison to other optimization technique, the reader is referred to [59].

To diversify exploration-exploitation balance, variants of PSO have been proposed. One of such variants is the flock of starlings optimization (FSO). Originally inspired by works on the collective behavior of birds [60], FSO introduces couplings between subsets of the particles composing the swarm [61], [62]. The right hand side of (26) and (27) is modified, including the additional terms [62]:

$$\tilde{v}_i = v_i + \frac{r_v}{n_i} \sum_{n \in N_i} v_n \quad (28a)$$

$$\tilde{\mu}_i = \mu_i + \frac{r_\mu}{n_i} \sum_{n \in N_i} \mu_n \quad (28b)$$

The additional terms describe a coupling between the i -th particle of the swarm and n_i other particles, belonging to the set N_i . The parameters r_v and r_μ are coupling weights. The coupling does not need to be topological, in the sense that, in general, it is not related to a “distance” relationship. Taking inspiration from bird flocks, the coupling is interpreted as a kinship relationship, creating network behaviors in the swarm.

VI. RESULTS

We have applied the PSO described in algorithm 1, to the optimization of a networked energy harvester with two, three and four mechanical degrees of freedom (DoF), respectively. The goal function to be maximized is the average harvested power P_{GL} given by (14), where the transfer function is given by (18a), and the transmission matrix is found using (19)-(23).

Figure 11 shows six examples of trajectories of PSO, for the energy harvester with two mechanical DoF. The two mechanical DoF was chosen because it allows for a clear visualization of trajectories in the parameter space S . The figure shows the average harvested power as a function of the inductance L_1 , and of the capacity C_1 . In the optimization the second inductance was fixed to $L_2 = 10.0$ mH and the capacitance to $C_2 = 1$ mF, to make a fair comparison with the single degree-of-freedom system. For reference, the average output power has been calculated using a grid search algorithm, shown in the figure as the background color. The trajectories of 20 particles, chosen at random between the 50 composing the swarm, are shown. It can be seen that the trajectories start from different random initial locations, and converge after few iterations to the same point of the parameter space, representing the maximum of the goal function. The convergence is very quick, requiring only few iterations. Table 3 summarizes the parameters’ values used for the PSO.

Figure 12 presents six examples of FSO trajectories. Each particle in the swarm – interpreted as a “bird” in the flock – is connected to seven “relatives” ($n_i = 7$).

TABLE 3. Parameters for PSO.

Parameter	Value
Cognitive coefficient: c_1	0.25
Social coefficient: c_2	0.25
Inertia weight: w	0.5
Swarm size: n_s	50
max iterations: t_{max}	100
Termination threshold: ϵ	10^{-8}

The coupling strengths for both position and velocity are set to $r_v = r_\mu = 0.3$ (see (28)). As in PSO, the trajectories eventually converge to the maximum of the goal function. However, the inter-bird coupling in FSO significantly alters the dynamics. While in PSO particles begin converging immediately, in FSO particles initially move along nearly parallel paths, mimicking the coordinated flight of a real flock. Only after this initial phase do they rapidly converge to the optimum. This coordinated movement allows the flock to explore a broader region of the parameter space, thereby enhancing the algorithm’s exploration capability and reducing the risk of becoming trapped in local maxima.

Table 4 summarizes the parameters found through PSO for networked energy harvesters with up to four mechanical DoF, and the corresponding average scavenged power. It can be seen that increasing the number of mechanical DoF improves the power performance significantly, but offers diminishing returns. In particular, the increase in average harvested power offered by a structure with four stages is negligible with respect to the three stage structure, suggesting that increasing the number of mechanical DoF beyond three/four is not worth the additional complexity.

The results presented in Table 4 demonstrate that, after proper optimization, the four DoF energy harvester generates more than 100% additional power compared to the single mechanical DoF energy harvester. This substantial increase in harvested power demonstrates the efficacy of the proposed solution. Swarm intelligence algorithms, including Multi-Objective Particle Swarm Optimization and Non-dominated Sorting Genetic Algorithm, have demonstrated comparable performance for other types of energy harvesters. For example, in [63], the authors achieved approximately 77.5% increases in harvested power. However, it should be noted that these methods pursued dual objectives – maximizing harvested power while simultaneously minimizing structural weight – which inherently limits the power optimization potential compared to our focused approach. It is worth noting that the proposed solution, schematically represented in Fig. 2, presents certain practical implementation challenges. The multi-DoF configuration may be difficult to implement in space-constrained environments or setups with geometric limitations. The increased mechanical complexity is expected to lead to higher manufacturing costs and a potential reduction in reliability, particularly under harsh operating conditions.

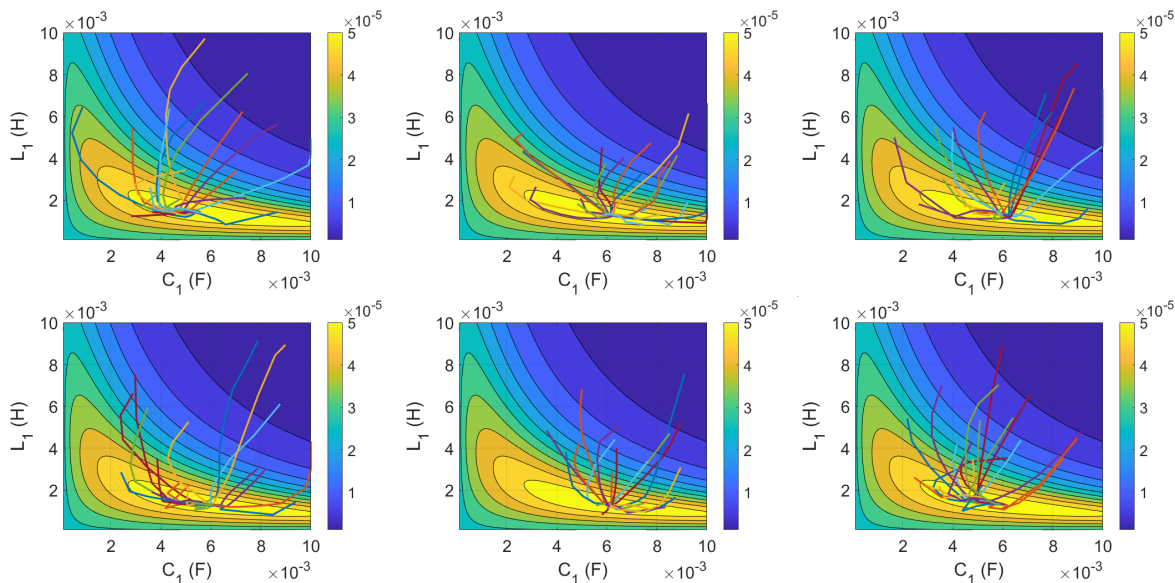


FIGURE 11. Six examples of trajectories in the parameter space for PSO of a networked energy harvester with two mechanical DoF. Parameters used for the optimization are summarized in table 3.

TABLE 4. Average harvested power and optimum values of the free parameters.

DoF	P_{out}	Parameters
1	28.74 μ W	$L = 10$ mH $C = 1$ mF
2	53.70 μ W	$L_1 = 1.30$ mH $L_2 = 10.0$ mH $C_1 = 6.0$ mF $C_2 = 1$ mF
3	58.15 μ W	$L_1 = 0.70$ mH $L_2 = 2.60$ mH $L_3 = 10.0$ mH $C_1 = 10.0$ mF $C_2 = 3.10$ mF $C_3 = 1$ mF
4	58.33 μ W	$L_1 = 0.7$ mH $L_2 = 2.0$ mH $L_3 = 1.0$ mH $L_4 = 10.0$ mH $C_1 = 9.0$ mF $C_2 = 1.0$ mF $C_3 = 1.9$ mF $C_4 = 1$ mF

It is interesting to compare the results obtained from PSO for the white Gaussian noise source, with the standard method for broadband impedance matching at a specific frequency ω . For the sake of simplicity, we consider the harvester with two and three mechanical DoF. The equivalent circuits are shown in Fig. 13, where the matching network corresponding to the additional mechanical DoF is highlighted by the square. The equivalent impedance of the last mass-spring pair, the piezoelectric transducer and the electrical load is

$$Z_{eq} = \left(j\omega L_n + \frac{1}{j\omega C_n} \right) + \frac{1}{n^2(j\omega C_{pz} + G_L)} \quad (29)$$

At the resonance frequency, the impedance is real $Z_{eq} = R_{eq} \in \mathbb{R}$. Using the parameters' values summarized in table 2, we obtain a resonance frequency $f_0 = 55.66$ Hz, and $R_{eq} = 0.1656 \Omega > R$.

For the single stage impedance matching network shown in Fig. 13(a), the quality factor is

$$Q = \sqrt{\frac{R_{eq}}{R}} - 1 \quad (30)$$

The elements of the matching network are given by:

$$L_1 = \frac{QR}{\omega} = 0.23 \text{ mH} \quad C_1 = \frac{Q}{\omega R_{eq}} = 11.7 \text{ mF} \quad (31)$$

and the harvested power is $P_{GL} = 34.33 \mu$ W.

For the two-stage matching network we introduce the virtual resistor $R_v = \sqrt{RR_{eq}}$. The quality factor is

$$Q = \sqrt{\frac{R_v}{R}} - 1 = \sqrt{\frac{R_{eq}}{R}} - 1 \quad (32)$$

The elements of the matching network are:

$$L_1 = \frac{QR}{\omega} = 0.158 \text{ mH} \quad L_2 = \frac{QR_v}{\omega} = 0.185 \text{ mH} \\ C_1 = \frac{Q}{\omega R_v} = 9.3 \text{ mF} \quad C_2 = \frac{Q}{\omega R_L} = 7.9 \text{ mF} \quad (33)$$

The corresponding harvested power is $P_{GL} = 34.16 \mu$ W.

Figure 14 shows a comparison of the amplitude response (the magnitude of the transfer function vs frequency) for the equivalent circuit with parameters determined by PSO, as summarized in table 4, and the parameters given by (31) and (33), respectively. On the left we show the amplitude response for the harvester with two mechanical DoF, while on the right for three DoF. The figure makes apparent how PSO operates, trading maximum amplitude at the resonance frequency for a larger bandwidth.

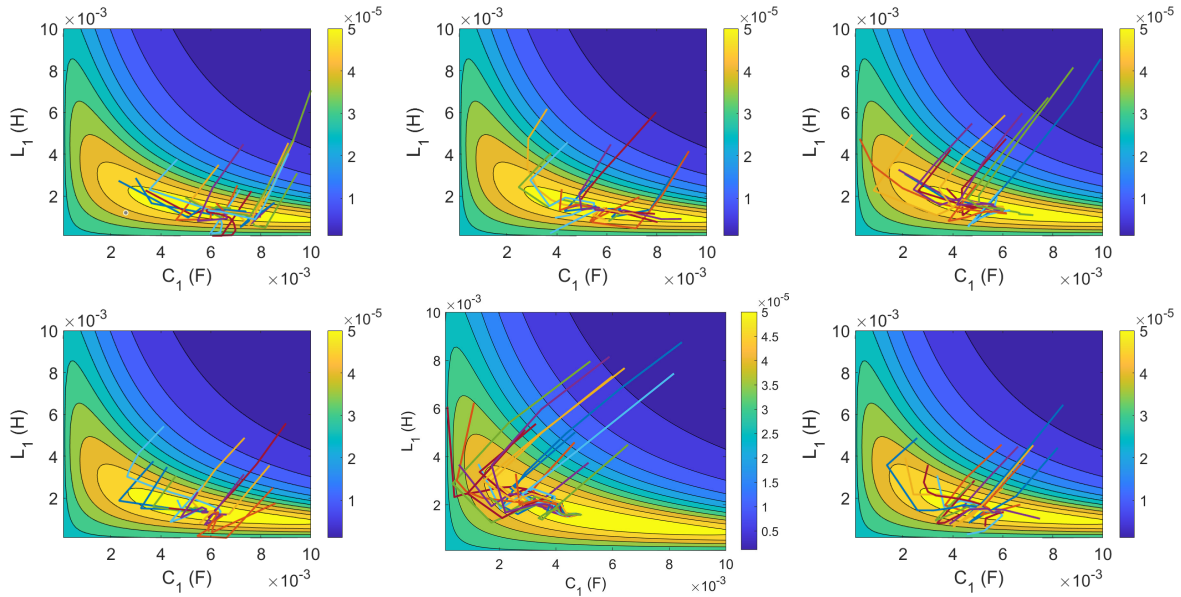


FIGURE 12. Six examples of trajectories in the parameter space for FSO of a networked energy harvester with two mechanical DoF. Parameters used in the optimization are the same used for PSO. Each “bird” is connected to seven relatives. Coupling strengths are $r_v = r_\mu = 0.3$.

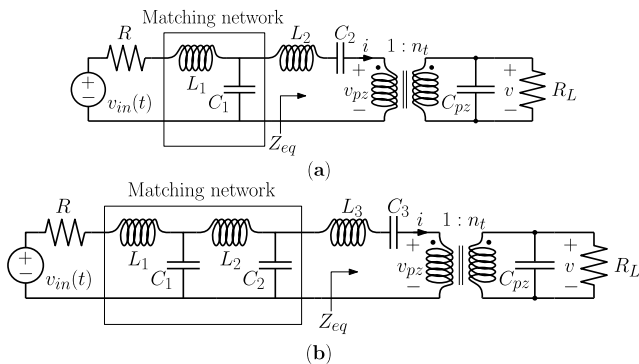


FIGURE 13. Equivalent circuits for the energy harvester with a one stage (part (a)) and two stages (in (b)) matching networks.

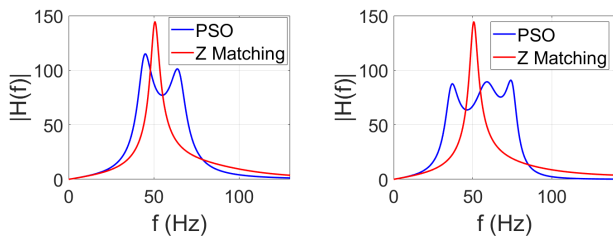


FIGURE 14. Amplitude response for the networked energy harvester with two (left) and three (right) mechanical DoF.

Finally, Fig. 15 shows a comparison of the optimized amplitude responses for the harvesters with one, two and three mechanical DoF. Again, the figure illustrates that the additional DoF permit to achieve a wider frequency bandwidth. The efficiency of energy collection at the resonance frequency is reduced but, in exchange, more energy is collected at neighbor frequencies.

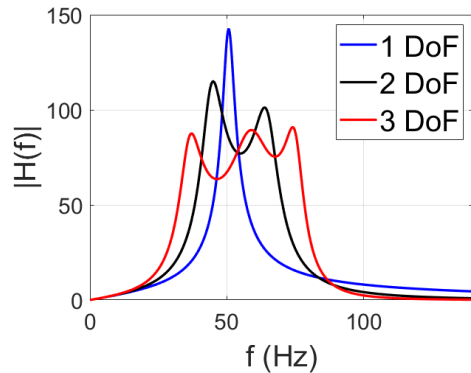


FIGURE 15. Amplitude response for the networked energy harvester with one, two, and three mechanical DoF.

VII. CONCLUSION

In this paper, we have introduced a networked energy harvester for ambient dispersed mechanical vibrations, based on a chain of coupled mechanical resonators. The harvester is schematically represented as a chain of masses connected in pairs by elastic springs, functioning as a mechanical filter. The masses and spring constants can be optimized to maximize either the scavenged energy or the power efficiency.

Ambient vibrations are modeled as white Gaussian noise. This is a reasonable model for vibrations arising from a large number of independent sources, and which frequency spectrum is wide enough. The kinetic energy from these vibrations is collected by the mass-spring system and converted into electrical power by a piezoelectric transducer.

The equations of motion for the electromechanical system are derived from equilibrium of forces. Using mechanical-to-

electrical analogies, an equivalent circuit for the harvester is presented. The circuit is analyzed in the frequency domain using transmission matrix formalism, and integral equations for the average harvested power and power efficiency are derived.

Finally, we consider the problem of the energy harvester optimization. Since the harvested power is described by an integral equation, the objective function and its derivatives are not directly available. Thus, gradient-free optimization methods are better suited for solving this problem. We employ particle swarm optimization to determine the optimal parameters of the equivalent circuit that maximize the average scavenged power. A comparison with conventional broadband filter design at a specific frequency shows that particle swarm optimization outperforms the classical method.

Our analysis demonstrates that adding a few mass-spring pairs significantly increases the average harvested power, overcoming limitations of previous approaches based on electrical impedance matching. In particular, the networked energy harvester with three mechanical DoF harvests 100% additional power compared to the single mechanical DoF harvester. We also show that further increasing the number of DoF offers negligible increases in scavenged power.

Finally, we reveal the mechanism through which increasing the number of degrees of freedom enhances harvested power. The networked harvester scavenges less power at the resonance frequency, but significantly enlarges the operational bandwidth. Thus, increasing the number of degrees of freedom enables the realization of a broadband filter that scavenges substantially more power by collecting energy across a wider frequency range. We demonstrate that broadband optimization using Particle Swarm Optimization achieves superior performance compared to analytical methods based on broadband impedance matching designed at the resonance frequency.

REFERENCES

- [1] S. P. Beeby, M. J. Tudor, and N. M. White, "Energy harvesting vibration sources for microsystems applications," *Meas. Sci. Technol.*, vol. 17, no. 12, pp. R175–R195, Dec. 2006.
- [2] A. Erturk and D. J. Inman, *Piezoelectric Energy Harvesting*. Hoboken, NJ, USA: Wiley, 2011.
- [3] J. A. Paradiso and T. Starner, "Energy scavenging for mobile and wireless electronics," *IEEE Pervasive Comput.*, vol. 4, no. 1, pp. 18–27, Jan. 2005.
- [4] Y.-W. Chong, W. Ismail, K. Ko, and C.-Y. Lee, "Energy harvesting for wearable devices: A review," *IEEE Sensors J.*, vol. 19, no. 20, pp. 9047–9062, Oct. 2019.
- [5] T. Sanislav, G. D. Mois, S. Zeadally, and S. C. Folea, "Energy harvesting techniques for Internet of Things (IoT)," *IEEE Access*, vol. 9, pp. 39530–39549, 2021.
- [6] M. Ujihara, G. P. Carman, and D. G. Lee, "Thermal energy harvesting device using ferromagnetic materials," *Appl. Phys. Lett.*, vol. 91, no. 9, Aug. 2007, Art. no. 093508.
- [7] Y. K. Tan and S. K. Panda, "Energy harvesting from hybrid indoor ambient light and thermal energy sources for enhanced performance of wireless sensor nodes," *IEEE Trans. Ind. Electron.*, vol. 58, no. 9, pp. 4424–4435, Sep. 2011.
- [8] F. Erkmen, T. S. Almonneef, and O. M. Ramahi, "Electromagnetic energy harvesting using full-wave rectification," *IEEE Trans. Microw. Theory Techn.*, vol. 65, no. 5, pp. 1843–1851, May 2017.
- [9] R. Sun, S. Zhou, Z. Li, and L. Cheng, "Dual electromagnetic mechanisms with internal resonance for ultra-low frequency vibration energy harvesting," *Appl. Energy*, vol. 369, Sep. 2024, Art. no. 123528.
- [10] J. Margielewicz, D. Gaska, T. Haniszewski, G. Litak, P. Wolszczak, M. Borowiec, P. Sosna, O. Ševeček, O. Rubeš, and Z. Hadaš, "Vibration energy harvesting system with cyclically time-varying potential barrier," *Appl. Energy*, vol. 367, Aug. 2024, Art. no. 123384.
- [11] L. Gammaitoni, I. Neri, and H. Vocca, "Nonlinear oscillators for vibration energy harvesting," *Appl. Phys. Lett.*, vol. 94, no. 16, Apr. 2009, Art. no. 164102.
- [12] A. Mitura, M. Brunetti, L. Kloda, F. Romeo, and J. Warminski, "Experimental nonlinear dynamic regimes for energy harvesting from cantilever bistable shells," *Mech. Syst. Signal Process.*, vol. 206, Jan. 2024, Art. no. 110890.
- [13] T. Chen, K. Wang, L. Cheng, H. Pan, H. Cui, and J. Zhou, "Theoretical and experimental research on a quasi-zero-stiffness-enabled nonlinear piezoelectric energy harvester," *Commun. Nonlinear Sci. Numer. Simul.*, vol. 133, Jun. 2024, Art. no. 107863.
- [14] S. Basaran, "Hybrid energy harvesting system under the electromagnetic induced vibrations with non-rigid ground connection," *Mech. Syst. Signal Process.*, vol. 163, Jan. 2022, Art. no. 108198.
- [15] X. Wang, T. Wang, H. Lv, H. Wang, and F. Zeng, "Analytical modeling and experimental verification of a multi-DOF spherical pendulum electromagnetic energy harvester," *Energy*, vol. 286, Jan. 2024, Art. no. 129428.
- [16] A. Sarviha, E. Barati, M. R. Zarkak, J. F. Derakhshandeh, and M. M. Alam, "Experimental investigations on the wake-induced vibration of an electromagnetic energy-harvesting system," *Int. J. Energy Res.*, vol. 2024, no. 1, Jan. 2024, Art. no. 7072340.
- [17] G. Wang, R. Song, L. Luo, P. Yu, X. Yang, and L. Zhang, "Multi-piezoelectric energy harvesters array based on wind-induced vibration: Design, simulation, and experimental evaluation," *Energy*, vol. 300, Aug. 2024, Art. no. 131509.
- [18] A. Erturk, J. Hoffmann, and D. J. Inman, "A piezomagnetoelastic structure for broadband vibration energy harvesting," *Appl. Phys. Lett.*, vol. 94, no. 25, Jun. 2009, Art. no. 254102.
- [19] Z. Yan, W. Sun, M. R. Hajji, W. Zhang, and T. Tan, "Ultra-broadband piezoelectric energy harvesting via bistable multi-hardening and multi-softening," *Nonlinear Dyn.*, vol. 100, no. 2, pp. 1057–1077, Apr. 2020.
- [20] I.-H. Kim, H.-J. Jung, B. M. Lee, and S.-J. Jang, "Broadband energy-harvesting using a two degree-of-freedom vibrating body," *Appl. Phys. Lett.*, vol. 98, no. 21, May 2011, Art. no. 214102.
- [21] H. Wu, L. Tang, Y. Yang, and C. K. Soh, "A novel two-degrees-of-freedom piezoelectric energy harvester," *J. Intell. Mater. Syst. Struct.*, vol. 24, no. 3, pp. 357–368, Feb. 2013.
- [22] W. Q. Zhu, G. Q. Cai, and R. C. Hu, "Stochastic analysis of dynamical system with double-well potential," *Int. J. Dyn. Control*, vol. 1, no. 1, pp. 12–19, Mar. 2013.
- [23] Y. Fu, H. Ouyang, and R. B. Davis, "Nonlinear dynamics and triboelectric energy harvesting from a three-degree-of-freedom vibro-impact oscillator," *Nonlinear Dyn.*, vol. 92, no. 4, pp. 1985–2004, Jun. 2018.
- [24] W. Sun, H. Jang, and J. Seok, "Magnetically coupled piezoelectric galloping-based energy harvester using a tandem configuration," *Mech. Syst. Signal Process.*, vol. 161, Dec. 2021, Art. no. 107952.
- [25] X. Li, J. Meng, C. Yang, H. Zhang, L. Zhang, and R. Song, "A magnetically coupled electromagnetic energy harvester with low operating frequency for human body kinetic energy," *Micromachines*, vol. 12, no. 11, p. 1300, Oct. 2021.
- [26] M. Bonnin, F. L. Traversa, and F. Bonani, "Leveraging circuit theory and nonlinear dynamics for the efficiency improvement of energy harvesting," *Nonlinear Dyn.*, vol. 104, no. 1, pp. 367–382, Mar. 2021.
- [27] M. Bonnin, F. L. Traversa, and F. Bonani, "An impedance matching solution to increase the harvested power and efficiency of nonlinear piezoelectric energy harvesters," *Energies*, vol. 15, no. 8, p. 2764, Apr. 2022.
- [28] M. Bonnin and K. Song, "Frequency domain analysis of a piezoelectric energy harvester with impedance matching network," *Energy Harvesting Syst.*, vol. 10, no. 1, pp. 135–144, Jan. 2023.
- [29] K. Song, M. Bonnin, F. L. Traversa, and F. Bonani, "Stochastic analysis of a bistable piezoelectric energy harvester with a matched electrical load," *Nonlinear Dyn.*, vol. 111, no. 18, pp. 16991–17005, Sep. 2023.
- [30] K. Song, M. Bonnin, F. L. Traversa, and F. Bonani, "Broadband vibration energy harvesting using nonlinear multi degree-of-freedom mechanical filters," *Nonlinear Dyn.*, vol. 113, no. 12, pp. 14301–14317, Jun. 2025.

- [31] D. S. Weile, E. Michielssen, and D. E. Goldberg, "Genetic algorithm design of Pareto optimal broadband microwave absorbers," *IEEE Trans. Electromagn. Compat.*, vol. 38, no. 3, pp. 518–525, Mar. 1996.
- [32] M. Ghoujani, M. Ravanbod, and S. Ebrahimi-Nejad, "Genetic-algorithm-assisted design of chiral honeycomb membrane acoustic metamaterials for broadband noise suppression," *J. Intell. Mater. Syst. Struct.*, vol. 35, no. 18, pp. 1426–1443, Nov. 2024.
- [33] M. Bonnini, K. Song, F. L. Traversa, and F. Bonani, "Model order reduction and stochastic averaging for the analysis and design of micro-electro-mechanical systems," *Nonlinear Dyn.*, vol. 112, no. 5, pp. 3421–3439, Mar. 2024.
- [34] K. Song, M. Bonnini, F. L. Traversa, and F. Bonani, "A stochastic averaging mathematical framework for design and optimization of nonlinear energy harvesters with several electrical DOFs," *Commun. Nonlinear Sci. Numer. Simul.*, vol. 139, Dec. 2024, Art. no. 108306.
- [35] L. Costanzo, A. Lo Schiavo, A. Sarracino, and M. Vitelli, "Stochastic thermodynamics of a piezoelectric energy harvester model," *Entropy*, vol. 23, no. 6, p. 677, May 2021.
- [36] S. P. Beeby, R. N. Torah, M. J. Tudor, P. Glynn-Jones, T. O'Donnell, C. R. Saha, and S. Roy, "A micro electromagnetic generator for vibration energy harvesting," *J. Micromech. Microeng.*, vol. 17, no. 7, pp. 1257–1265, Jul. 2007.
- [37] B. P. Mann and N. D. Sims, "Energy harvesting from the nonlinear oscillations of magnetic levitation," *J. Sound Vibrat.*, vol. 319, nos. 1–2, pp. 515–530, Jan. 2009.
- [38] S.-D. Kwon, J. Park, and K. Law, "Electromagnetic energy harvester with repulsively stacked multilayer magnets for low frequency vibrations," *Smart Mater. Struct.*, vol. 22, no. 5, May 2013, Art. no. 055007.
- [39] F. Cottone, P. Basset, H. Vocca, L. Gammaitoni, and T. Bourouina, "Bistable electromagnetic generator based on buckled beams for vibration energy harvesting," *J. Intell. Mater. Syst. Struct.*, vol. 25, no. 12, pp. 1484–1495, Aug. 2014.
- [40] K. Kucab, G. Górski, and J. Mizia, "Energy harvesting in the nonlinear electromagnetic system," *Eur. Phys. J. Special Topics*, vol. 224, nos. 14–15, pp. 2909–2918, Nov. 2015.
- [41] G. Caruso, S. Galeani, and L. Menini, "Semi-active damping and energy harvesting using an electromagnetic transducer," *J. Vibrat. Control*, vol. 24, no. 12, pp. 2542–2561, Jun. 2018.
- [42] L. Costanzo, A. Lo Schiavo, A. Sarracino, and M. Vitelli, "Stochastic thermodynamics of an electromagnetic energy harvester," *Entropy*, vol. 24, no. 9, p. 1222, Aug. 2022.
- [43] L. Wang and F. G. Yuan, "Vibration energy harvesting by magnetostrictive material," *Smart Mater. Struct.*, vol. 17, no. 4, Aug. 2008, Art. no. 045009.
- [44] C. S. Clemente, D. Davino, and V. P. Loschiavo, "Analysis of a magnetostrictive harvester with a fully coupled nonlinear FEM modeling," *IEEE Trans. Magn.*, vol. 57, no. 6, pp. 1–4, Jun. 2021.
- [45] C. S. Clemente, D. Davino, I. Iannone, and V. P. Loschiavo, "Experimental characterization of an AC–DC boost for energy harvesting device based on magnetostrictive materials," *Electricity*, vol. 5, no. 1, pp. 24–35, Jan. 2024.
- [46] S. Boisseau, G. Despesse, and B. T. Ahmed, "Electrostatic conversion for vibration energy harvesting," in *Small-Scale Energy Harvesting*. London, U.K.: InTech, May 2012.
- [47] E. Lefeuvre, A. Badel, C. Richard, L. Petit, and D. Guyomar, "A comparison between several vibration-powered piezoelectric generators for standalone systems," *Sens. Actuators A, Phys.*, vol. 126, no. 2, pp. 405–416, Feb. 2006.
- [48] W. J. Choi, Y. Jeon, J.-H. Jeong, R. Sood, and S. G. Kim, "Energy harvesting MEMS device based on thin film piezoelectric cantilevers," *J. Electroceram.*, vol. 17, nos. 2–4, pp. 543–548, Dec. 2006.
- [49] K. A. Cook-Chennault, N. Thambi, and A. M. Sastry, "Powering MEMS portable devices—A review of non-regenerative and regenerative power supply systems with special emphasis on piezoelectric energy harvesting systems," *Smart Mater. Struct.*, vol. 17, no. 4, Aug. 2008, Art. no. 043001.
- [50] S. Priya, H.-C. Song, Y. Zhou, R. Varghese, A. Chopra, S.-G. Kim, I. Kanno, L. Wu, D. S. Ha, J. Ryu, and R. G. Polcawich, "A review on piezoelectric energy harvesting: Materials, methods, and circuits," *Energy Harvesting Syst.*, vol. 4, no. 1, pp. 3–39, Aug. 2019.
- [51] C. Covaci and A. Gontean, "Piezoelectric energy harvesting solutions: A review," *Sensors*, vol. 20, no. 12, p. 3512, Jun. 2020.
- [52] C. Z. Rosen, B. V. Hiremath, and R. Newnham, *IEEE Standard on Piezoelectricity*, ANSI/IEEE Standard 176-1987, 1988, pp. 227–228.
- [53] S. Priya and D. J. Inman, *Energy Harvesting Technologies*. Cham, Switzerland: Springer, 2009.
- [54] C. W. Gardiner, *Handbook of Stochastic Methods*, vol. 3. Berlin, Germany: Springer, 1985.
- [55] K. Rajwar, K. Deep, and S. Das, "An exhaustive review of the algorithms for search and optimization: Taxonomy, applications, and open challenges," *Artif. Intell. Rev.*, vol. 56, no. 11, pp. 13187–13257, Nov. 2023.
- [56] J. Kennedy and R. C. Eberhart, "Particle swarm optimization," in *Proc. Int. Conf. Neural Netw.*, vol. 4, Apr. 2002, pp. 1942–1948.
- [57] T. M. Shami, A. A. El-Saleh, M. Alswaiti, Q. Al-Tashi, M. A. Summakieh, and S. Mirjalili, "Particle swarm optimization: A comprehensive survey," *IEEE Access*, vol. 10, pp. 10031–10061, 2022.
- [58] M. Clerc and J. Kennedy, "The particle swarm—explosion, stability, and convergence in a multidimensional complex space," *IEEE Trans. Evol. Comput.*, vol. 6, no. 1, pp. 58–73, Jan. 2002.
- [59] M. J. Kochenderfer and T. A. Wheeler, *Algorithms for Optimization*. Cambridge, MA, USA: MIT Press, 2019.
- [60] M. Ballerini, N. Cabibbo, R. Candelieri, A. Cavagna, E. Cislani, I. Giardina, V. Lecomte, A. Orlandi, G. Parisi, A. Procaccini, M. Viale, and V. Zdravkovic, "Interaction ruling animal collective behavior depends on topological rather than metric distance: Evidence from a field study," *Proc. Nat. Acad. Sci. USA*, vol. 105, no. 4, pp. 1232–1237, Jan. 2008.
- [61] F. R. Fulginei and A. Salvini, "The flock of starlings optimization: Influence of topological rules on the collective behavior of swarm intelligence," in *Studies in Computational Intelligence*, 2010, pp. 129–145.
- [62] N. Netjinda, T. Achalakul, and B. Sirinaovakul, "Particle swarm optimization inspired by starling flock behavior," *Appl. Soft Comput.*, vol. 35, pp. 411–422, Oct. 2015.
- [63] M. Momen, S. Ebrahimi-Nejad, and M. Mollajafari, "Multi-objective optimization of exponential-cross-section piezoelectric cantilever under tire rotational excitation for self-powered tire pressure monitoring systems," *J. Cleaner Prod.*, vol. 500, Apr. 2025, Art. no. 145255.



MICHELE BONNINI received the Laurea degree in physics from the Università di Torino, Turin, Italy, in 2003, and the Ph.D. degree in electronics and communications engineering from the Politecnico di Torino, Turin, in 2007.

He joined the Department of Electronics and Telecommunications, Politecnico di Torino, in 2011, as an Assistant Professor. He has been an Associate Professor with the Politecnico di Torino, since 2017. He has held visiting researcher positions with the Laboratoire de Mathématiques Appliquées, Université du Havre, Le Havre, France, and with the Institute for Information and Communication Technologies, Electronics and Applied Mathematics, Université Catholique de Louvain, Louvain-la-Neuve, Belgium. Since 2024, he has been a Visiting Professor with the TTPU—Turin Polytechnic University in Tashkent, Uzbekistan. He is the author or co-author of more than 100 papers published in international journals and conference proceedings. His research interests include nonlinear dynamics, complex systems, stochastic processes, and their applications to both classical and quantum circuits and systems.

Prof. Bonnini received the Best Paper of the Year Award from *International Journal of Circuit Theory and Applications*, in 2004.



KAILING SONG (Member, IEEE) received the bachelor's degree in mechanical engineering from Tianjin Polytechnic University, China, in 2016, the master's degree in mechanical engineering from Tianjin University, China, in 2019, and the Ph.D. degree in sustainable development and climate change from the IUSS–School for Advanced Studies, Pavia, Italy, in 2024.

In 2024, she was a Visiting Researcher with the Nonlinear Dynamics Group, Institute for Mechanical Systems, ETH Zurich, Switzerland. Since November 2024, she has been a Postdoctoral Researcher with the Department of Electronics and Telecommunications, Politecnico di Torino, Turin, Italy. Her doctoral research focused on the application of nonlinear dynamics and circuit theory to the development of innovative solutions for energy harvesting. Her research interests include nonlinear circuit modeling, simulation and theoretical analysis, stochastic processes, and noise analysis in energy harvesting system design, as well as advanced simulation and numerical methods.



FABIO L. TRAVERSA received the Laurea degree in nuclear engineering and the Ph.D. degree in physics from the Politecnico di Torino, Turin, Italy, in 2004 and 2008, respectively.

He is currently the Co-Founder and the Chief Technology Officer with MemComputing Inc., the deep-tech company he launched with physicist Max Di Ventra and entrepreneur John Beane, in 2016. Before MemComputing, he was a Research Scientist with the University of California San Diego, where his work on unconventional computing sparked the invention of memcomputing technology. He has also held academic positions as a Visiting Professor with the Politecnico di Torino and a Research Fellow with the Universitat Autònoma de Barcelona, Barcelona, Spain. An author of more than 100 peer-reviewed publications, he holds several national and international patents covering hardware designs for unconventional computing and artificial intelligence. He is internationally recognized for his contributions to electronics, physics, and advanced computing paradigms. His research interests include memcomputing, theoretical and solid-state physics, dynamical systems, noise in electronic circuits and devices, energy harvesting, machine learning, AI hardware, and FPGA development.



FABRIZIO BONANI (Senior Member, IEEE) was born in Turin, Italy, in 1967. He received the Laurea (cum laude) and Ph.D. degrees in electronic engineering from the Politecnico di Torino, Turin, in 1992 and 1996, respectively.

Since 1995, he has been with the Department of Electronics, Politecnico di Torino, where he is currently a Full Professor of electronics. He is the author or co-author of more than 250 papers published in international journals and conference proceedings. His main research interests include the physics-based simulation of semiconductor devices, with special emphasis on the noise analysis of field-effect and bipolar transistors, the thermal analysis of power devices and circuits, and the simulation and design of power semiconductor devices. He is also interested in the stability analysis of nonlinear circuits and systems, noise analysis of nonlinear circuits, and the modeling and design of linear and nonlinear energy harvesters. He is a member of the MTT-14 Technical Committee on Low-Noise Techniques. He has been on the Technical Program Review Committee for the International Microwave Symposium, since 2013. He was an Associate Editor of IEEE TRANSACTIONS ON COMPUTER-AIDED DESIGN OF INTEGRATED CIRCUITS AND SYSTEMS. He is an Associate Editor of IEEE TRANSACTIONS ON ELECTRON DEVICES and IEEE TRANSACTIONS ON MICROWAVE THEORY AND TECHNIQUES.

...